Absolute surface energies of group-IV semiconductors: Dependence on orientation and reconstruction

A. A. Stekolnikov, J. Furthmüller, and F. Bechstedt
Institut für Festkörpertheorie und Theoretische Optik, Friedrich-Schiller-Universität, 07743 Jena, Germany
(Received 13 July 2001; revised manuscript received 23 October 2001; published 28 February 2002)

We use a plane-wave-pseudopotential code to study the surface energetics for the elemental semiconductors Ge, Si, and diamond from *first principles*. Various reconstruction geometries including 1×1, 2×1, $c(4\times2)$, $c(2\times8)$, and 7×7 of the low-index surfaces (100), (110), and (111) are optimized with respect to the atomic coordinates. The resulting total energies are related to the accompanying band structures. Chemical trends are derived. The different reconstruction behavior is discussed in terms of atomic sizes and orbital energies.

DOI: 10.1103/PhysRevB.65.115318 PACS number(s): 68.35.Bs, 68.35.Md, 73.20.At, 61.50.Ah

I. INTRODUCTION

The absolute value of the surface free energy of a crystalline solid is one of the most important fundamental quantities which characterizes a large number of basic and applied phenomena. Among them are crystal growth, surface faceting, growth of thin layers, and the shape of small crystallites. One of the fascinating problems concerns the equilibrium shape of nanocrystallites fabricated from group-IV materials germanium (Ge), silicon (Si), and perhaps also diamond (C). The formation of self-assembled islands or quantum dots, during the epitaxial growth of Ge on Si(100) (Refs. 1 and 2) and Si on α-SiC(0001),[3] is characterized by several distinct island shapes and an unusual island size distribution. Predeposited C atoms may have a substantial influence on the dot formation.[4] There is an evolution of the shape of Si/Ge nanocrystallites on Si(100). Depending on the crystallite volume, a shape transition from pyramids to domes is observed.[5,6]

Apart from a knowledge of the strain state, the construction of the crystal shape requires a complete determination of the surface free energy γ as a function of the surface orientation **n**. Despite its importance, there are few experimental data concerning surface free energies because they are difficult to measure. Using a cleavage technique, Gilman[7] measured the energy of the Si(111) surface. A study of the equilibrium shape of voids in silicon allowed one to extract the surface energies for three further orientations [100], [311], and [110].[8] Theoretical data are also rather rare. A fully quantum-mechanical treatment usually only gives relative surface energies for different reconstructions but for one and the same orientation. Calculations of absolute surface energies are mainly restricted to semiempirical methods such as the tight-binding approach,[9] or to the use of classical interaction potentials.[10,11] Values obtained from first-principles calculations are only available for 1×1 and 2×1 reconstructions of diamond surfaces,[12–14] as well as for Si(111) and (100) surfaces.[15–17]

A particular deficit of the measurements and calculations is the neglect of a consideration of the surface reconstruction. However, reconstruction plays a significant role for the semiconductors considered. It is now generally accepted that the (100) surfaces of diamond, silicon, and germanium show dimer-based reconstructions.[18,19] At room temperature, Si and Ge exhibit a 2×1 reconstruction governed by asymmetric dimers (AD's).[20] A staggered arrangement of these dimers explains the $c(4\times2)$ low-temperature phase of Si(100).[19] Symmetric dimers (SD's) dominate the 2×1 reconstruction of the C(100) surface.[21] The topography of a clean (110) surface is somewhat different from that of a (111) surface with step structures. Rather, it is represented by long-range reconstructions, e.g., 16×2.[22,23] On the other hand, a study within the 1×1 translational symmetry should give the basic structural and electronic features of such surfaces. The two atoms in a corresponding unit cell are allowed to relax, i.e., to form pairs or chains and, hence, to possess occupied and empty surface bands in the region of the fundamental gap as in the case of III-V(110)1×1 surfaces.[24]

The (111) surfaces of diamond, silicon, and germanium show a manifold and puzzling reconstruction behavior.[25] The (111) surfaces of silicon and germanium exhibit a 2×1 reconstruction following cleavage at room temperature. However, such a reconstruction can also be found on the C(111)2×1 surface.[19] From many experimental and theoretical studies, the (111) surfaces are believed to have a π-bonded chain geometry.[26] In the case of Si and Ge, the π-bonded chains are tilted,[27–29] whereas converged total-energy calculations do not indicate either a chain buckling or a chain dimerization for diamond(111).[30–32,12] There is only one exception among the predictions.[33] For Si and Ge, the π-bonded reconstruction has two different isomers with the tilt angle of the uppermost chains in opposite directions.[29,34,35] The chain-left isomer of the π-bonded chains was indeed observed by means of scanning tunneling microscopy (STM).[36] Heat treatments of cleaved Si(111) and Ge(111) surfaces at elevated temperatures cause the 2×1 reconstruction to convert to the 7×7 [Si (Ref. 37)] and the $c(2\times8)$ [Ge (Ref. 38)] structures, respectively. Whereas the Si(111)7×7 surface is now explained by a dimer-adatom-stacking-fault (DAS) model with corner holes,[39,40,15,16] the Ge(111)$c(2\times8)$ surface can be represented by a simple adatom model.[41,42] Recently, it was shown that a $c(2\times8)$ reconstruction can be also observed on the quenched Si(111) surface.[43,44]

In this paper, we report on the results of *ab initio* total-energy minimization and electronic-structure calculations

based on the parameter-free pseudopotential-plane-wave method for all the materials, surface orientations, and reconstructions mentioned above. The organization of the paper is as follows: Section II is devoted to a description of the computational methods. It is described how converged values can be obtained for absolute surface energies. The results for the geometries, energies, and band structures are discussed in Sec. III. We report trends with the size of the group-IV atom and the surface orientation. Finally, a brief summary is presented in Sec. IV.

II. COMPUTATIONAL METHODS

A. Total and single-particle energies

The total energies and the underlying electronic band structures are calculated within the density functional theory (DFT) and the local-density approximation (LDA). Explicitly we use the VASP code.[45] The electron-ion interaction is treated by non-norm-conserving ultrasoft pseudopotentials of the Vanderbilt type.[46] They allow a fully quantum-mechanical treatment of several hundred atoms in the unit cell, in particular in the case of first-row elements like carbon with the lack of core p electrons.[47] The electron-electron interaction is described by the Ceperley-Alder functional as parametrized by Perdew and Zunger. As a consequence of the optimization of the pseudopotentials, the plane-wave expansions of the single-particle eigenfunctions are restricted to 19.8 Ry (C), 9.6 Ry (Si), and 8.8 Ry (Ge). The **k**-space integrals over the three- or two-dimensional Brillouin zones (BZ's) are approximated by sums over special points of the Monkhorst-Pack (MP) type.[48]

Our calculations employ the conjugate-gradient method to minimize the total energy of the system with respect to the atomic coordinates $\{\mathbf{R}_i\}$. When the Hellmann-Feynman forces are smaller than 10 meV/Å, the surface structure is considered to be in the equilibrium. The electronic band structures are plotted for the obtained equilibrium atomic coordinates. Quasiparticle corrections[49,50] are not taken into account. The method was carefully tested in the case of the large 3×3 reconstruction of SiC surfaces.[51–53] In the case of the diamond structure of the bulk group-IV materials, the lattice constants a and fundamental energy gaps E_g are $a=3.531$, 5.398, and 5.627 Å and $E_g=4.15$, 0.46, and 0.00 eV for C, Si, or Ge in the DFT-LDA quality. In the underlying computations we have used a mesh of $6\times6\times6$ MP grid points, i.e., a total of 28 **k** points in the irreducible part of the Brillouin zone of the fcc crystal structure.

B. Slab approximation and absolute surface energy

In order to model the various surfaces, we consider periodic arrangements of slabs along the surface normal. Each slab consists of a certain number of atomic layers. Within one supercell the number of atoms in one layer is restricted to the surface unit cell. The slabs are separated by sufficiently thick vacuum regions. In contrast to compound semiconductors, the group-IV materials possess the advantage that for the stacking directions [111] and [100] centrosymmetric supercells can also be constructed.

The two surfaces of a centrosymmetric slab are physically equivalent and, hence, allow a direct calculation of absolute surface energies. As an advantage, in the centrosymmetric case the same surface and, hence, the same surface reconstruction $n\times m$, occurs on both sides of a material slab. For a given atomic configuration $\{\mathbf{R}_i\}$ in such a slab the surface energy (per 1×1 surface cell) can directly be inferred from the total energy of the slab $E_{tot}(N,\{\mathbf{R}_i\})$ with N atoms by subtracting N times the bulk energy μ per atom:

$$E_{surf}^{n\times m}=\frac{1}{2nm}\{E_{tot}(N,\{\mathbf{R}_i\})-\mu N\}. \tag{1}$$

The introduction of the chemical potential μ of the constituents allows one to compare surfaces with different numbers of atoms in the two-dimensional surface unit cell. We use the calculated values $\mu=-5.195$, -5.957, and -10.147 eV for Ge, Si, and C. In the case of the primitive $n\times m$ reconstructions $n\times m$ gives the number of 1×1 unit cells. In the case of a centered structure $c(n\times m)$, this number has to be divided by a factor 2. The prefactor $\frac{1}{2}$ in expression (1) indicates that for centrosymmetric slabs two equivalent surfaces are involved in the calculations. The surface energy per unit area,

$$\gamma^{n\times m}=E_{surf}^{n\times m}/A, \tag{2}$$

immediately follows, dividing expression (1) by the area A of an 1×1 cell for a given surface orientation **n**.

The quality of the surface calculations depends on the number of atomic layers and vacuum layers used in a supercell of the repeated-slab approximation. We have performed convergence studies using slabs with 18, 15, or 24 atomic layers and 30, 27, or 36 vacuum layers for the (111), (110), or (100) surface orientation for all three materials.

In principle, relations (1) and (2) give the precise expressions applicable to arbitrary surface translational symmetries and reconstruction models. However, despite the consideration of nonpolar group-IV semiconductors, the numerical effort due to the use of centrosymmetric slabs becomes too large. Too many atoms have to be taken into account for a converged calculation. This holds, in particular, for large reconstructions like 7×7. For this reason we only use centrosymmetric slabs to obtain absolute surface energies for the unrelaxed surfaces with 1×1 translational symmetry.

In order to reduce the effort, we follow an idea developed for the polar (111) and (100) surfaces of compound semiconductors.[54] One surface of the slab is saturated with hydrogen atoms. The bottom layers of the hydrogen-covered slab sides are kept frozen during surface optimizations. They simulate the bulk regions of the semiconductors under consideration. Consequently, the numbers of the atomic layers (vacuum layers) are reduced to 8 (10), 15 (9), and 8 (8) for reconstructions of (111), (110), and (100) surfaces for all materials considered. The uppermost five atomic layers are allowed to relax. Only in the case of the (111)7×7 surfaces, determining the atomic geometries, do we restrict ourselves to six atomic layers covered by an incomplete layer of adatoms on the upper slab side and a hydrogen layer on the bottom side. However, with the resulting atomic coordinates the total-energy calculations have been repeated using eight

atomic layers to find converged surface energies. According to the idea of expression (1), for a given surface orientation one obtains the sum of two absolute surface energies,

$$E_{surf}^{n\times m}+E_{surf}^{H}=\frac{1}{n\cdot m}\{E_{tot}(N,N_H,\{\mathbf{R}_i\})-\mu N-\mu_H N_H\}: \tag{3}$$

one for the clean surface, $E_{surf}^{n\times m}$, and one for the hydrogen-covered surface, E_{surf}^{H}. Thereby, N_H denotes the number of hydrogen atoms, i.e., $N_H=n\times m$ in the case of the (111) orientation and $N_H=2n\times m$ for noncentered (110) and (100) surface reconstructions. The chemical potential μ_H of the hydrogen atoms varies depending on the reservoir. Here we assume that the reservoir is given by free hydrogen atoms, the total energy of which is taken from a calculation including spin polarization. As a consequence of the chosen H chemical potential, the energy values of the hydrogen-covered surfaces, E_{surf}^{H}, will be negative.

We explicitly compare results of calculations for centrosymmetric slabs [Eq. (1)] and one-sided H-covered slabs [Eq. (3)] in the case of unrelaxed surfaces and extract the absolute energy E_{surf}^{H} of the surfaces saturated by hydrogen. However, the calculations of the absolute surface energies for relaxed and reconstructed surfaces do not really need E_{surf}^{H}. Using expression (3), we only calculate the energy gain

$$\Delta E^{n\times m}=\frac{1}{n\cdot m}[E_{tot}(N_{ideal},N_H,\{\mathbf{R}_i\}) - E_{tot}(N_{n\times m},N_H,\{\mathbf{R}_i\})-\mu\Delta N] \tag{4}$$

per 1×1 cell of a relaxed or reconstructed surface with respect to the corresponding unrelaxed surface. The number $\Delta N=N_{ideal}-N_{n\times m}$ indicates the variation of the number of group-IV atoms in the slab, depending on the surface reconstruction. The noncentrosymmetric slabs with eight or 15 atomic layers are sufficient to calculate the energy gain $\Delta E^{n\times m}$ with a high accuracy of about 1 meV, whereas the absolute surface energies using such slab thicknesses in the symmetric case possess an inaccuracy of about 0.02 eV. The absolute surface energies, which are given in the following, are combined by the accurately calculated absolute surface energies of unreconstructed surfaces and energy gains due to reconstruction. They follow from the relation $E_{surf}^{n\times m}=E_{surf}^{1\times1}(\text{unrelaxed})-\Delta E^{n\times m}$.

C. BZ sampling

The **k**-point sampling in the irreducible part of the BZ varies with the orientation and reconstruction of the surface. In the case of the (111) orientation we use the following dense grids of Monkhorst-Pack points: $8\times8\times1$ for 1×1, $4\times8\times1$ for 2×1, $4\times4\times1$ for $c(2\times8)$, and $2\times2\times1$ for 7×7. These grids correspond to 20 (1×1), 8 (2×1), 6 [$c(2\times8)$], and 2 (7×7) **k** points in the irreducible part of the surface BZ. In the case of unreconstructed (110)1×1 surfaces, the **k**-point sampling is replaced by 24 points in the irreducible part of the BZ. This corresponds to a $(8\times6\times1)$ grid of Monkhorst-Pack points. Three different reconstructions are considered for the (100) surfaces. $(8\times8\times1)$, $(4\times8\times1)$, and $(2\times4\times1)$ grids are used for the 1×1, 2×1, and $c(4\times2)$ reconstructions. In the irreducible part of the BZ there are 16 (1×1), 8 (2×1), and 2 [$c(4\times2)$] **k** points. The **k**-point meshes and slab thicknesses used give rise to extremely accurate results. Useful test quantities are the resulting chemical potentials of the bulk materials. After filling the vacuum regions by atoms in bulk positions, we calculate chemical potentials μ which only vary by maximum deviations from the ''bulk'' values of 2.2, 0.7, or 0.2 meV for Ge, Si, and C, with the slab orientation and size of the two-dimensional unit cell. Moreover, the different **k**-point sets are only used to calculate the reconstruction-induced energy gains $\Delta E^{n\times m}$.

III. RESULTS AND DISCUSSION

A. Energetics

The results for the absolute surface energies are listed in Table I. The (111) surfaces are indeed the cleavage faces of group-IV semiconductors crystallizing in diamond structure. This holds for comparison of both unrelaxed and relaxed/reconstructed situations. All considered rearrangements of surface atoms—the relaxed 1×1 surface,[19] the π-bonded chain model of a 2×1 surface with the two isomers,[29,34] the $c(2\times8)$ adatom reconstruction,[41,42] and the 7×7 DAS model[15,16,39,40]—give rise to local minima on the total-energy surface. The (111) surface gains energy during relaxation or reconstruction. The gain values obtained from other *ab initio* calculations[12,28–32] for relaxed 1×1 and π-bonded chain 2×1 surfaces are rather similar. This holds, for example, for the remarkable large energy gain due to relaxation of the C(111) surface, which has been traced back to a tendency for the formation of a graphite overlayer.[31] There is also agreement concerning the favorization of the chain-left isomer for Ge.[29,35] The situation is less clear in the Si case, since the energy differences between chain-right and chain-left isomers are smaller, in agreement with Refs. 34 and 35.

Table I clearly indicates the different reconstruction behavior of the three group-IV semiconductors under consideration.[25] According to our calculations, we find a further lowering of the absolute surface energy going from the 2×1 reconstruction (the π-bonded chain model) to the $c(2\times8)$ reconstruction (the adatom model) and 7×7 (the DAS model) in the case of both Ge and Si. In the case of diamond the large reconstructions are completely unfavorable. This is in agreement with recent studies,[55] which found that adatoms and vacancies on the diamond(111) surface are energetically less favorable than the relaxed surface in contrast to the case of Si and Ge. For instance, the truncated diamond crystal gains more energy by the relaxation in the first atomic layers than by the addition of adatoms leading to a $c(2\times8)$ translational symmetry. The increase of the energy gain in the Ge(111)$c(2\times8)$ and Si(111)7×7 cases with respect to the 2×1 surface is in agreement with previous calculations.[29,42] Here we also clearly show that in the Si case the 7×7 reconstruction (the DAS model) gives the most favorable reconstruction. In the Ge case, we observe more or less the same energy for $c(2\times8)$ and 7×7. This may be a consequence of

TABLE I. Absolute surface energies $E_{surf}^{n\times m}$ and $\gamma^{n\times m}$ for various orientations and reconstructions.

Orientation	Reconstruction	E_{surf} (eV/1×1 cell)			γ(J/m^2)		
		C	Si	Ge	C	Si	Ge
(111)	unrelaxed	2.735	1.435	1.128	8.12	1.82	1.32
	relaxed	2.165	1.372	1.116	6.43	1.74	1.30
	2×1(right)	1.369	1.141	0.901	4.06	1.45	1.05
	2×1(left)	1.369	1.136	0.893	4.06	1.44	1.04
	$c(2\times8)$	2.346	1.109	0.864	6.96	1.41	1.01
	7×7	2.395	1.073	0.872	7.11	1.36	1.02
	H-covered	−2.760	−2.383	−2.249	−8.19	−3.03	−2.63
(110)	unrelaxed	4.115	2.630	2.127	7.48	2.04	1.51
	relaxed	3.264	2.190	1.661	5.93	1.70	1.17
	H-covered	−5.496	−4.644	−4.637	−9.99	−3.61	−3.32
(100)	unrelaxed	3.780	2.174	1.691	9.72	2.39	1.71
	relaxed	3.655	2.173	1.690	9.40	2.39	1.71
	2×1	2.222	1.321	1.035	5.71	1.45	1.05
	$c(4\times2)$	2.222	1.285	0.985	5.71	1.41	1.00
	H-covered	−3.545	−4.853	−4.525	−9.11	−5.34	−4.56

numerical inaccuracies, related in particular to the small number of atomic layers used in the calculation. In contrast to Ref. 25, the energy values in Table I are really calculated with eight atomic layers and 16 vacuum layers in the supercell. This give rise to a favorization of $c(2\times8)$ versus 7×7 in the Ge case. On the other hand the 7×7 surface can be also prepared for germanium in the presence of biaxial strain.[56] It is also not clear whether the favorization of $c(2\times8)$ against 2×1 in the Si case is a real effect or a consequence of numerical inaccuracies due to the use of different **k**-point samplings. In any case, a $c(2\times8)$ ordering is observed on the quenched Si(111) surface.[43] We mention that the energy gain of 0.26 eV due to the adatom adsorption between $c(2\times8)$ and 1×1 (relaxed) is close to the adatom binding energy measured by means of STM on Ge(111).[57]

Even in the 1×1 case, where no reconstruction is allowed, the (110) surface gains energy by a mixed bond-contraction and bond-rotation mechanism. The bonds of the zigzag chains in the first-atomic layer are slightly shortened. In the case of Si and Ge these chains are additionally buckled. The energy gain varies slightly between C, Si, and Ge. However, instead considering the absolute numbers, the surface energy decreases.

In the case of the (100) face, relaxation only gives a negligible energy gain. The surface energies are substantially lowered, allowing a dimerization of two surface atoms accompanied by a 2×1 reconstruction. We calculate huge reconstruction energies of about 1.6, 0.9, and 0.6 eV for C, Si, or Ge due to the formation of dimers. Whereas the dimers on C(100)2×1 are symmetric, they exhibit a remarkable asymmetry on Si and Ge(100). A staggered arrangement of the buckled dimers in a $c(4\times2)$ reconstruction slightly lowers the Si and Ge surface energies further.

The absolute surface energies are very interesting. They show a clear chemical trend going from C to Si, and Ge, similar to the bulk cohesive energies. In general, the largest surface energies appear for the diamond surfaces, whereas the smallest ones are calculated for germanium. The surface energies E_{surf} for the 1×1 and 2×1-reconstructed diamond surfaces are in complete agreement with results of previous first-principles calculations.[12–14] On the other hand, computations using classical interaction potentials underestimate the surface energies with γ=3.39 (unrelaxed) and 0.83 (relaxed) J/m^2 (Ref. 10) in the case of diamond with strong bonds. In the Si case this underestimation is less drastical. The method using interaction potentials[10] gives 1.15 and 1.02 J/m^2. A molecular dynamics simulation with empirical potentials[11] ends with a value γ=1.41 J/m^2 for the relaxed Si(111)1×1 surface, whereas tight-binding calculations[9] also lead to γ=1.41 J/m^2, but for a 2×1-reconstructed surface. Previous *ab initio* calculations reported a value of 1.13 J/m^2 for 2×1 reconstruction.[17] Experimentally surface energies for Si(111) were extracted from the equilibrium shape of voids as γ=1.23 J/m^2.[8] Using a cleavage technique, Gilman[7] measured a surface energy of Si(111) as 1.24 J/m^2 at a low temperature of −196 °C. These experimental values are close to the theoretical ones calculated for reconstructed surfaces. We have to mention that with 1.51 and 1.18 eV Stich *et al.*[16] and Brommer *et al.*[15] calculated values for E_{surf} which envelope the surface energy of Si(111)7×7 given in Table I. However, the energy lowering (0.06 eV) of Stich *et al.*[16] for 7×7 with respect to 2×1 exactly approaches the value obtained here. To our knowledge, neither experimental nor theoretical values have been published in the case of germanium.

In the case of the (110) and (100) orientations the situation for the comparison of the values in Table I and published theoretical and experimental values is similar to that for the (111) surfaces. The values γ=1.36,[8] 1.34,[9] and 1.72 J/m^2 (Ref. 11) were published for the Si(110)1×1 surface. For the (100) orientation one finds, for Si surfaces with unspecified

or 2×1 reconstructions, the values $\gamma=1.36$,[8] 1.34,[9] 1.49,[11] and 1.16 J/m^2 (Ref. 17). Other calculations[10] give $\gamma=2.32$ and 1.21 J/m^2 for the unrelaxed or relaxed surface. Huge values are reported for diamond(100). Classical potentials give the values $\gamma=9.21$ and 3.34 J/m for the unrelaxed or relaxed surfaces.[9,10] The huge reduction of the surface energy per unit area due to surface relaxation agrees with the *ab initio* findings listed in Table I.

The surface energies measured for Si exhibit orderings of (111), (100) and (110).[8] This is in disagreement with the findings in Table I for both unrelaxed and relaxed faces. It therefore indicates a considerable influence of the surface reconstruction. Only after inclusion of a 7×7 reconstruction of the (111) face and a $c(4\times2)$ reconstruction of the (100) face and we find an energetic ordering with the sequence (111), (100), and (110). The (111) surface is indeed the cleavage face. For the unrelaxed stage the energetical ordering according to γ is along the (111), (110), and (100) surfaces. After inclusion of the relaxation, but keeping the 1×1 translational symmetry, even the (110) face becomes energetically favorable. This tendency seems to be in agreement with the empirical fact that the relaxed (110) surface is the cleavage face for compound semiconductors.[19] The situation is similar for diamond. The (110) orientation seems to be more favorable than the (111) one. Only after allowing a surface reconstruction does the (111) face become the face with the lowest surface energy. The picture is less clear for germanium because of a tendency toward a vanishing orientation dependence of the surface energies as a consequence of the weaker bonds. In the relaxed and unrelaxed cases the same energetical ordering as for silicon is observed. However, in contrast to Si and C, the absolute surface energies of the reconstructed (111) and (100) faces approach each other. Even values $\gamma_{100}=1.00$ J/m^2 and $\gamma_{111}=1.01$ J/m^2 are calculated after a consideration of the $c(4\times2)$ and $c(2\times8)$ reconstructions. However, their difference of 0.01 J/m^2 comes within the range of the accuracy of the calculations. In particular, the huge buckling amplitude of the Ge dimers in the (100) case and the accompanying energy gain may be slightly overestimated using the LDA for exchange and correlation.

The surface energies E_{surf}^{H} of the hydrogenated surfaces are always lower than the surface energies $E_{surf}^{n\times m}$ of the corresponding most stable reconstructed surfaces (see Table I). The adsorption energy $E_{ads}^{H}=E_{surf}^{n\times m}-E_{surf}^{H}$ per hydrogen atom is always larger than the molecular binding energy per atom of the hydrogen molecule 2.45 eV. Consequently, a dissociative adsorption of H_2 on all the considered surfaces should be possible, unless there is a large barrier in the entrance channel.

B. Geometry

In Table II we list values of the characteristic geometry parameters for the various reconstructions of the (111) faces, but also give several data for the two other surface orientations considered. All lengths are given in units of the corresponding theoretical bulk bond length: $d_{bulk}=1.529$, 2.337, and 2.436 Å. The geometry parameters are introduced in Fig. 1. The parameter l characterizes the distance between the nominal first- and second-atomic layers on the relaxed (111) surface. In the case of the $c(2\times8)$ adatom reconstruction and the 7×7 DAS model, l gives the vertical distances between rest atoms (l_{rest}), adatoms (l_{ad}), center-corner-hole atoms (l_{corner}), and atoms in the layer below. For the rest atoms and the adatoms, we list an average value in Table II independent of the atomic position and the faulted or unfaulted area in the 7×7 cell. We only distinguish between the rest atoms on the faulted and the unfaulted regions. In Table II we list the triple values of l, etc., since on the ideal surfaces with atoms in bulklike positions and bulk bond lengths these vertical distances are given by $d_{bulk}/3$. With the exception of l_{ad} for $c(2\times8)$, the values of the vertical distances on the (111) surfaces indicate a completely different behavior of diamond on the one hand and silicon or germanium on the other hand. For diamond these distances are usually smaller than $d_{bulk}/3$, indicating a strong tendency for graphitization in the first atomic layers. This vertical approach of atoms in neighboring atomic layers is particularly well pronounced for the relaxed surface. In this case Si and Ge(111)1×1 surfaces also exhibit a small approach of first- and second atomic layers. However, for $c(2\times8)$ and 7×7 reconstructions the adatoms, rest atoms, and corner-hole Si or Ge atoms show the opposite effect. For Si and Ge(111)$c(2\times8)$, one observes an increase of l_{rest} with respect to the ideal value, whereas the adatoms are displaced toward the bulk. This geometry is accompanied by a rehybridization of the rest atoms, resulting in *s*-like dangling bonds. Consequently, the adatoms should donate their electrons to the *s*-like dangling bonds of the rest atoms resulting in an energy gain. The adatoms on the $c(2\times8)$ surface and 7×7 surface in T_4 position are characterized by a bond length d_{ad} to the atoms in the nominal first-atomic layer. Interestingly, this parameter practically does not vary with the group-IV semiconductor, neither in the $c(2\times8)$ case nor in the 7×7 case. The adatom heights l_{ad} above the first-atomic layer depend on the area in the 7×7 case. We confirm the experimental and theoretical result for Si (Refs. 59–62) that l_{ad} is larger for the faulted region than for the unfaulted region. However, this effect (not shown in Table II) is more pronounced for Ge than for Si. The opposite behavior occurs for the rest atoms. In the 7×7 DAS case, we also consider the dimer bond length d_{dim}, which, however, also does not vary with the element. Another interesting parameter is the vertical distance D of the adatoms to the second atomic layer. It almost approaches the value of the bulk bond length, indicating the basic idea of the T_4 adatoms that the wave functions of adatoms and second-layer atoms overlap.

The chain-right and chain-left isomers of the 2×1 π-bonded chain reconstruction are characterized by a bond length d_{chain} and the buckling Δz of the chains. A possible dimerization of the chains on the (111) surface is not indicated. The bonds along π-bonded chains are slightly contracted with respect to the ideal bulk bond length found by many authors. There is a clear chemical trend. The contraction is the largest one for diamond. We confirm the remarkable buckling of the chains on the Si and Ge(111)2×1 surfaces[29,34,35] and its vanishing value for C(111)2×1.[12,31,32] Bond contraction and buckling are rather independent of the

TABLE II. Characteristic geometry parameters of relaxed or reconstructed (111) surfaces. In the (110) and (100) cases the consideration is restricted to a relaxed 1×1 surface and a dimerized 2×1 reconstruction, respectively. All lengths are given in units of the bulk bond length. The dimer buckling is characterized by the angle φ (in degrees). Average values are given for inequivalent adatoms or rest atoms.

Reconstruction	Geometry parameter	Diamond	Silicon	Germanium
(111)1×1 (relaxed)	$3l$	0.50	0.79	0.90
(111)2×1 (right)	Δz	−0.00	0.23	0.34
	d_{chain}	0.93	0.97	0.99
(111)2×1 (left)	Δz	0.00	0.27	0.34
	d_{chain}	0.93	0.97	0.99
(111)$c(2\times8)$ (adatom)	$3l_{ad}$	0.58	0.55	0.58
	d_{ad}	0.88	0.86	0.88
	D	1.04	1.03	1.07
	$3l_{rest}$	0.75	1.41	1.51
	d_{rest}	0.72	0.81	0.83
(111)7×7 (DAS)	$3l_{ad}$	1.75	1.67	1.75
	d_{ad}	1.06	1.05	1.07
	$3l_{rest}$ (faulted)	0.72	1.41	1.50
	$3l_{rest}$ (unfaul.)	0.72	1.35	1.50
	d_{rest}	0.98	1.02	1.03
	$3l_{corner}$	0.88	1.44	1.56
	d_{dim}	1.08	1.04	1.04
(110)1×1	Δz	0.00	0.33	0.34
(relaxed)	d_{chain}	0.93	0.99	1.00
(100)2×1	d_{dim}	0.90	0.98	1.00
(AD)	d_{back}	1.03	1.02	1.03
	d'_{back}	1.03	0.99	1.00
	φ	0	18.4	20.4

chain-right or chain-left isomer. Only the buckling increases from the chain-right to the chain-left isomer of Si(111)2×1.

The (110) cleavage surfaces of zinc-blende crystals conserve the bulk-terminated 1×1 translational symmetry. The relaxation is characterized by a bond-rotation model or a bond-contraction model depending on the strength and ionicity of the bonds.[58] First-layer atoms with a dangling bond are arranged in weakly interacting zigzag chains along the

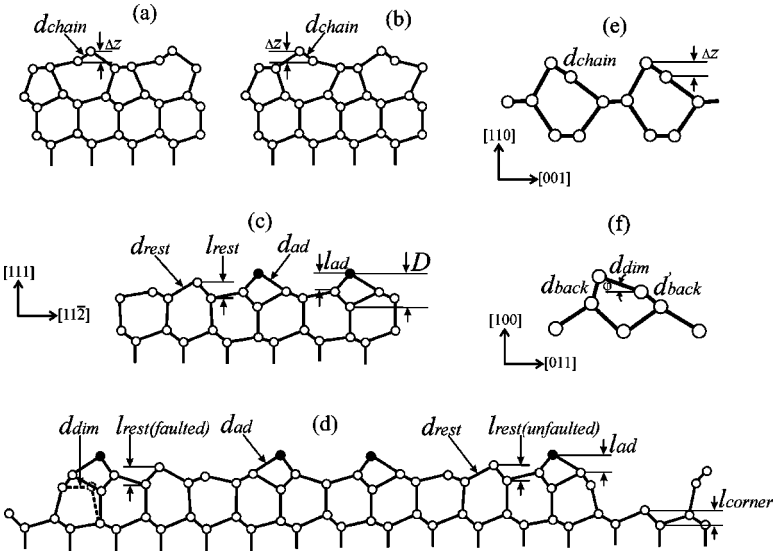

FIG. 1. Side views of surface reconstructions of group-IV semiconductors. (a) π-bonded chain model of (111)2×1, chain-right isomer; (b) π-bonded chain model of (111)2×1, chain-left isomer; (c)(111)$c(2\times8)$, adatom model; (d) (111)7×7, DAS model; (e) (110)1×1, relaxed; (f) (100)2×1, asymmetric dimer model. The geometry parameters used in the text and in Table II are indicated. In addition, in (d) the dimer length is also indicated. Filled circles in (c) and (d) represent adatoms.

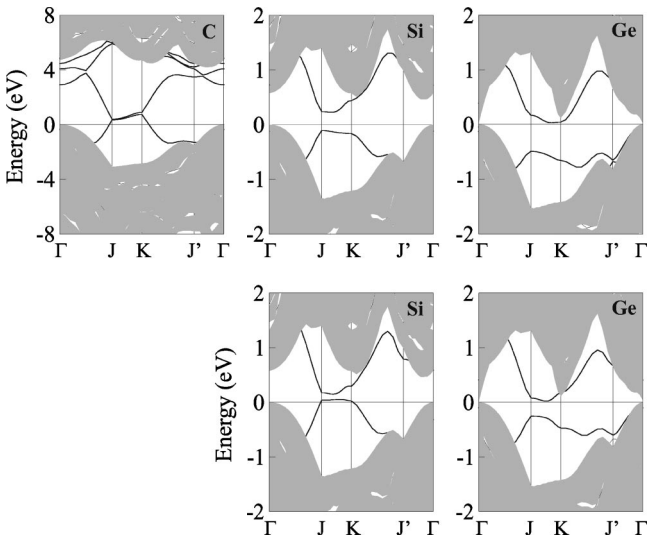

FIG. 2. Band structures of the (111)2×1 surfaces described within the π-bonded chain model. The upper panels show the bands of the chain-right isomers, whereas the lower panels give the results for the chain-left isomers.

$[\bar{1}10]$ direction. These chains are characterized by a bond length d_{chain} and a buckling Δz of the two atoms in a 1×1 unit cell. Basically the same relaxation types occur in the case of the group-IV elements. Table II shows that in the diamond-structure case the Si and Ge(110)1×1 surfaces are clearly described by the bond-rotation mechanism. The bulk bond lengths are conserved, but substantial chain bucklings are observed. Diamond(110)1×1 exhibits the opposite behavior, i.e., it is characterized by a bond-contraction relaxation mechanism. There is no buckling but a remarkable shortening of the chain bonds.

The basic 2×1 reconstruction of the (100) surfaces also indicates an opposite behavior of silicon and germanium, on the one hand and diamond, on the other hand. Dimers with strong bonds are formed. Their bond lengths d_{dim} are close to the bulk ones for Si and Ge (cf. Table II) but d_{dim} approaches the value of a double bond >C═C< in the diamond case. In the latter case the dimers are symmetric, whereas Si and Ge show asymmetric dimers. This asymmetry is well characterized by the different lengths d_{back} and d'_{back} of the backbonds of the two dimer atoms. The tilt angles φ of the Si and Ge dimers are, at about 20°, rather large, but are in agreement with other *ab initio* calculations.[20]

C. Band structures

The different geometries influence the band structures. Their occupied parts may, however, give an explanation of the energetics discussed above. This relationship will be demonstrated for the 2×1, $c(2\times8)$, and 7×7 reconstructions of the (111) surfaces, as well as for the relaxed (110)1×1 and dimerized (100)2×1 surfaces discussed in Figs. 2, 5, and 6, and Fig. 1 of Ref. 25. All these figures show the projected bulk band structures as shaded regions in the surroundings of the fundamental gap. Solid lines represent the surface bands. Certain high-symmetry directions are chosen in the corresponding surface BZ.[63] The valence-band maximum (VBM) of the bulk band structure is taken as energy zero.

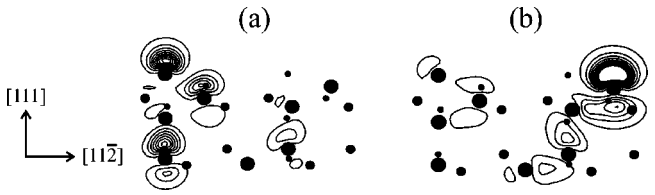

FIG. 3. Contour plots of surface states of the Ge(111)$c(2\times8)$ surface. The wave-function squares are represented in a (110) plane. (a) State of the lowest empty surface band at a wave vector on the ΓY line (cf. Fig. 1 of Ref. 25), mainly localized at a T_4 adatom. (b) State of the highest occupied surface band close to the VBM at a wave vector at the $\Gamma Y'$ line, mainly localized at a rest atom. The distance of the Ge atoms to the plane of adatom and rest atom is indicated by varying size of the dots.

The band structures of the π-bonded chain reconstructions in Fig. 2 along the $\Gamma J-JK-KJ'-J'\Gamma$ directions are characterized by an upper π^*-like band and a lower π-like band in the fundamental bulk energy gap. In the diamond case the surface is metallic within the DFT-LDA employed. The two bands are degenerate at J in the surface BZ. Moreover, both bands widely overlap in energy along the JK direction. The chain buckling in the case of the Si and Ge atoms with larger cores lifts the band degeneracy. The corresponding surfaces become insulating. A small indirect energy gap appears along the JK line. This splitting is smaller for the chain-left isomers. This fact is accompanied by a slightly higher-energy position of the occupied π band in the chain-left case. This does not allow us to explain the energetic favorization of the chain-left structure, in particular in the case of germanium, simply by an energy gain due to the band structure energy. Perhaps the changed topology of the fivefold and sevenfold rings in the layers beneath plays a role. On the other hand, the alignment of the projected bulk band structure and the slab band structure may be accompanied by an inaccuracy of the surface band positions by about 0.1 eV.

The band structures of the $(111)c(2\times8)$ surfaces are plotted in Fig. 1 of Ref. 25 along the high-symmetry directions $\Gamma Y\text{-}YY'\text{-}Y'\Gamma$ in the BZ of the two-dimensional c-rectangular Bravais lattice.[63] Essentially the dangling bonds belonging to the two adatoms and the two rest atoms appear in the fundamental gap region of the projected bulk band structure. The wave functions of two of these bands are represented in Fig. 3. The four bands are clearly observable for diamond because of the weak interaction of the dangling bonds and the similarities of the adatom and rest atom bonding to the underlying atomic layer (cf. Table II). There is only a vanishing surface-state gap. In the silicon case the adatom dangling bonds become more p_z-like, whereas the rest atom dangling bonds increase the s character. As a consequence, surface bands belonging to the rest atoms are close to the VBM of the bulk band structure and, hence, completely filled with electrons. A remarkable gap occurs between the empty and filled dangling-bond states localized at adatoms or rest atoms. In the Ge case, the occupied rest atom bands are further shifted into the projected bulk valence

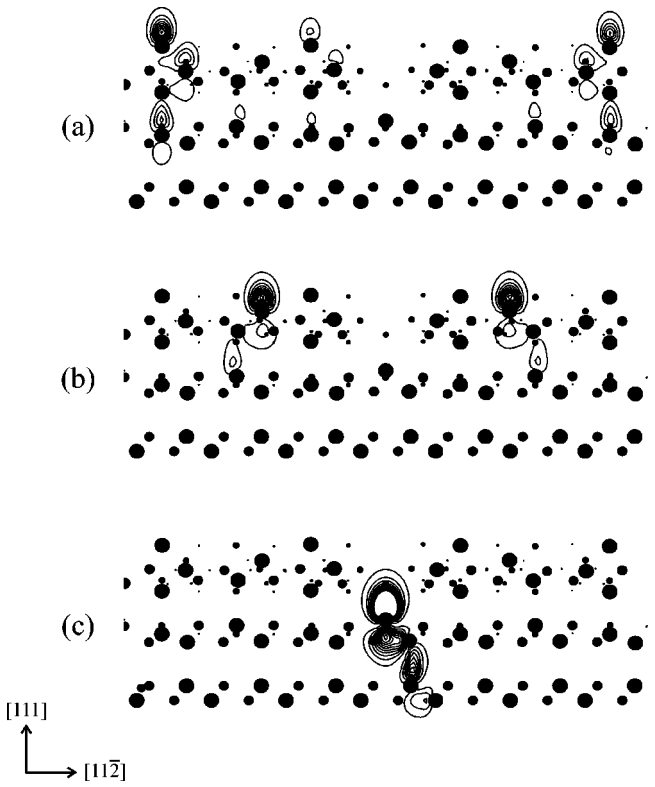

FIG. 4. Contour plots of surface states of the Si(111)7×7 surface. The wave function squares are represented in a (110) plane for surface bands plotted in Fig. 1 of Ref. 25 (a) Partially filled surface band in the gap. (b) Occupied slab band just below the VBM. (c) Occupied surface band above the VBM.

bands. The accompanying energy gain via the band structure energy explains why the $c(2\times8)$ reconstruction is energetically more favorable than the π-bonded chain 2×1 reconstruction, as well as why this happens in particular for germanium.

The band structures of the (111)7×7 surfaces were already represented in Fig. 1 of Ref. 25 along a high-symmetry direction in the twodimensional hexagonal BZ. Here we mainly discuss the electronic structure for silicon. We observe several occupied, half-occupied, and empty surface bands within the fundamental gap of the projected bulk band structure. They belong to the dangling bonds situated at the adatoms, rest atoms, and corner-hole atoms.[64] Corresponding selected states are represented in Fig. 4. Within the DFT-LDA band structure of Si, the surface Fermi level is located at about 0.3 eV. The half-filled band that pins the Fermi level shows strong contributions from dangling bonds of adatoms. Dangling bonds localized at rest atoms and corner-hole atoms contribute to the occupied bands just below the Fermi level. The tendency that the occupied dangling bonds of the rest atoms dominate this region of surface states was also found by other authors.[64] The contribution of dangling bonds situated at adatoms near the corner holes or in the center of the unit mesh are much smaller. The empty surface bands mainly arise from the dangling bonds of adatoms. The interpretation of the states at the Ge(111)7×7 surface is more complicated, since the fundamental gap in the projected bulk

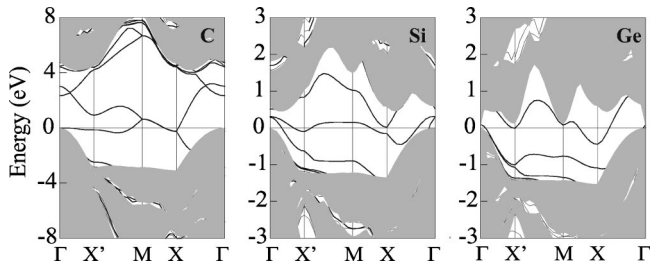

FIG. 5. Band structures of relaxed (110)1×1 surfaces.

band structure is so small in the DFT-LDA. Only a few surface bands really represent bound states. In the diamond case one observes a dense package of dangling-bond-derived bands. As a consequence of the weak geometrical changes, practically all types of dangling bonds contribute to the bunch of surface bands around the Fermi level in the center of the fundamental gap.

Figure 5 presents the bands of the clean relaxed (110)1×1 surfaces together with the projected bulk band structures. The two dangling bonds per surface unit cell lead to two bands, which are situated within the bulk fundamental gap. In the diamond case the two dangling bonds remain equivalent. Consequently the two bands degenerate along the MX line, i.e., perpendicular to the surface chain orientation. The bands split along the other BZ boundary MX'. Along the ΓX and $\Gamma X'$ directions the surface bands exhibit a remarkable dispersion. Nevertheless the C(110)1×1 surface is metallic. Along the row C→Si→Ge the chemical trend is similar to the (111)2×1 case. The chain buckling (cf. Table II) lifts the degeneracy of the two bands along MX. However, in the Si case the effect is not strong enough. The Si(110)2×1 surface becomes semimetallic. For Ge(110)2×1 a true surface-state gap is opened along the MX line. On the other hand, the bands are shifted toward the occupied bulk bands, and the uppermost band exhibits a strong dispersion as a consequence of the interchain interaction. It also results in a semimetallic surface electronic structure.

The surface electronic structures resulting within the SD or AD model of the (100)2×1 surfaces are plotted in Fig. 6. As a consequence of the π interaction, a bonding π band and an antibonding π^* band appear in the fundamental gap of the projected bulk band structure. The dimer-dimer interaction leads to a strong band dispersion along the JK and KJ' directions. Already within the SD model, the two surface bands are separated in the diamond case. For Si and Ge an insulating surface only occurs after dimer buckling. The cor-

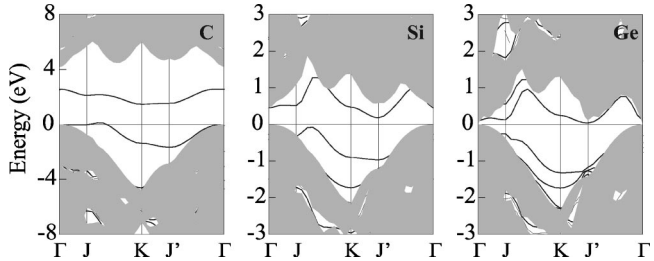

FIG. 6. Band structures of dimerized (100)2×1 surfaces.

responding energy gain via the band-structure energy explains why the symmetry-breaking tilting of the dimers is energetically favorable.

More precisely, we have to mention that the band structure of C(100)2×1 in Fig. 6 was calculated using symmetric slabs. The idea of saturation of the dangling bonds at one slab side by hydrogen atoms cannot be used to obtain a reliable band structure of C(100)2×1. Already for C(111)2×1, $c(2\times8)$ and 7×7, unphysical surface bands related to the antibonding C-H orbital combinations occur in the upper part of the fundamental gap close to the bulk conduction bands (cf. left panels in Figs. 2, and 5, but also in Fig. 1 of Ref. 25). However in the (100) case with two dangling bonds per surface atom the interaction of neighboring C-H antibonds is so strong that the fundamental gap is filled with hydrogen-related surface states. On the other hand, the idea that the group-IV hydrogen bonding and antibonding orbital combinations give rise to energies far away from the fundamental band gap is still valid for silicon and germanium. The above mentioned problems occur only in the diamond case because of the large fundamental gap.

IV. SUMMARY

In summary, we have presented rather complete first-principles studies of the energetics and the reconstruction of the low-index surfaces of the three group-IV semiconductors diamond, silicon, and germanium. The calculations have been performed within the DFT in the LDA and the slab approximation. More in detail, 1×1, 2×1, $c(4\times2)$, $c(2\times8)$, and 7×7 reconstructions have been investigated. The atomic geometries have been optimized to find the minimum of the total energy. For the atomic structures obtained, the band structures have also been calculated.

Absolute surface energies are needed to discuss the equilibrium shape of diamond, Si, and Ge crystals. A combination of symmetric slabs and slabs with a hydrogen passivation at one side allowed a determination of absolute surface energies not only for unreconstructed surfaces. Such a combination also makes the computations tractable and not too costly for reconstructed surfaces with large unit cells. In the case of the (111) orientation we found that the 2×1 reconstruction gives the lowest energy only for diamond. For Si and Ge the large 7×7 or $c(2\times8)$ reconstructions are energetically more favorable. A similar behavior occurs for the (100) surfaces. For Si and Ge the $c(4\times2)$ reconstructions are lower in energy than the 2×1 surface. In contrast, in the diamond case no asymmetric dimers occur at the (100) face.

The tendency toward stabilization of symmetric structures on diamond surfaces and the tendency toward symmetry reductions at the Si and Ge surfaces are observed not only for the (111)2×1 and (100)2×1 translational symmetries but also for the relaxed (110)1×1 faces. Any buckling of chains or dimers induces a substantial subsurface strain and, hence, makes a symmetry break unlikely in the diamond case. The tilting of chains and dimers on Si and Ge surfaces opens energy gaps between surface states. The accompanying energetical lowering of the occupied bands gives rise to an energy gain. Moreover, such a tilting allows different chain isomers on the Si and Ge(111) surfaces and the $c(4\times2)$ translational symmetry of the (100) surfaces of Si and Ge.

Our *ab initio* total-energy and electronic-structure results highlight the physical origins of the reconstruction behavior as it depends on the surface orientation and size of the group-IV atom. We have shown clear evidence of an opposite reconstruction behavior of diamond and Si or Ge surfaces. Adatoms and symmetry-breaking distortions are unlikely for diamond as a consequence of the short interatomic distances and strong bonds. However, such elements of the surface reconstruction occur on Si and Ge surfaces. The complicated interplay of bonding, the resulting atomic geometry, and the accompanying electronic structure have been derived, and used to discuss driving forces for the surface reconstruction.

ACKNOWLEDGMENTS

This work was been supported by the Deutsche Forschungsgemeinschaft (Sonderforschungsbereich 196, Project No. A8) and the EU Research Training network NANOPHASE (Contract HPRN-CT-2000-00167). We also thank the John von Neumann Institute for Computing (Forschungszentrum Jülich) for providing us with computational resources.

[1] D.J. Eaglesham and M. Cerullo, Phys. Rev. Lett. **64**, 1943 (1990).
[2] F.M. Ross, J. Tersoff, and R.M. Tromp, Phys. Rev. Lett. **80**, 984 (1998).
[3] A. Fissel, K. Pfennighaus, and W. Richter, Thin Solid Films **318**, 88 (1998).
[4] O.G. Schmidt, C. Lange, K. Eberl, O. Kienzle, and F. Ernst, Appl. Phys. Lett. **71**, 2340 (1997).
[5] G. Medeiros-Ribeiro, A.M. Bratkovski, T.I. Kamins, D.A.A. Ohlberg, and R.S. Williams, Science **279**, 353 (1998).
[6] F.M. Ross, R.M. Tromp, and M.C. Reuter, Science **286**, 1931 (1999).
[7] J.J. Gilman, J. Appl. Phys. **31**, 2208 (1960).
[8] D.J. Eaglesham, A.E. White, L.C. Feldman, N. Moriya, and D.C. Jacobson, Phys. Rev. Lett. **70**, 1643 (1993).
[9] J.H. Wilson, J.D. Todd, and A.P. Sutton, J. Phys.: Condens. Matter **2**, 10259 (1990); **3**, 1971 (1991).
[10] T. Takai, T. Halicioglu, and W.A. Tiller, Surf. Sci. **164**, 327 (1985).
[11] G.H. Gilmer and A.F. Bakker, in *Defects in Materials*, edited by P. O. Bristowe, J. E. Epperson, J. E. Griffith, and Z. Lilihenthal-Weber, Mater. Res. Soc. Symp. Proc. No. 209 (Materials Research Society, Pittsburgh, 1991), p. 135.
[12] G. Kern, J. Hafner, and G. Kresse, Surf. Sci. **366**, 445 + 464 (1996).
[13] G. Kern and J. Hafner, Phys. Rev. B **56**, 4203 (1997).
[14] J. Furthmüller, J. Hafner, and G. Kresse, Phys. Rev. B **53**, 7334 (1996).

[15] K.D. Brommer, M. Needels, B.E. Larson, and J.D. Joannopoulos, Phys. Rev. Lett. **68**, 1355 (1992).
[16] I. Stich, M.C. Payne, R.D. King-Smith, J.-S. Lin, and L.J. Clarke, Phys. Rev. Lett. **68**, 1351 (1992).
[17] S.C. Erwin, A.A. Baski, and L.J. Whitman, Phys. Rev. Lett. **77**, 687 (1996).
[18] D.J. Chadi, Phys. Rev. Lett. **43**, 43 (1979).
[19] W. Mönch, *Semiconductor Surfaces and Interfaces* (Springer, Berlin, 2001).
[20] P. Krüger and J. Pollmann, Phys. Rev. Lett. **74**, 1155 (1995).
[21] C. Kress, M. Fiedler, W.G. Schmidt, and F. Bechstedt, Phys. Rev. B **50**, 17697 (1994).
[22] Y. Ishikawa, Y. Hosakawa, I. Hamaguchi, and T. Ichinokawa, Surf. Sci. **187**, L606 (1987).
[23] Y. Yamamoto, T. Sueyoshi, T. Sato, and M. Iwatsuki, Surf. Sci. **466**, 183 (2000).
[24] J.L.A. Alves, J. Hebenstreit, and M. Scheffler, Phys. Rev. B **44**, 6188 (1991).
[25] F. Bechstedt, A.A. Stekolnikov, J. Furthmüller, and P. Käckell, Phys. Rev. Lett. **87**, 016103 (2001).
[26] K.C. Pandey, Phys. Rev. Lett. **47**, 1913 (1981); **49**, 223 (1982).
[27] J.E. Northrup and M.L. Cohen, Phys. Rev. Lett. **49**, 1349 (1982).
[28] J.E. Northrup, M.S. Hybertsen, and S.G. Louie, Phys. Rev. Lett. **66**, 500 (1991).
[29] N. Takeuchi, A. Selloni, A.I. Shkrebtii, and E. Tosatti, Phys. Rev. B **44**, 13611 (1991).
[30] B.N. Davidson and W.E. Pickett, Phys. Rev. B **49**, 11253 (1994).
[31] A. Scholze, W.G. Schmidt, and F. Bechstedt, Phys. Rev. B **53**, 13725 (1996).
[32] W.G. Schmidt, A. Scholze, and F. Bechstedt, Surf. Sci. **351**, 183 (1996).
[33] S. Iarlori, G. Galli, F. Gygi, M. Parrinello, and E. Tosatti, Phys. Rev. Lett. **69**, 2947 (1992).
[34] S.-H. Lee and M.-H. Kang, Phys. Rev. B **54**, 1482 (1996).
[35] M. Rohlfing, M. Palummo, G. Onida, and R. Del Sole, Phys. Rev. Lett. **85**, 5440 (2000).
[36] H. Hirayama, N. Sugihara, and K. Takayanagi, Phys. Rev. B **62**, 6900 (2000).
[37] R.E. Schlier and H.E. Farnsworth, J. Chem. Phys. **30**, 917 (1959).
[38] P.W. Palmberg and W.T. Peria, Surf. Sci. **6**, 57 (1967).
[39] K. Takayanagi, Y. Tanishiro, M. Takahashi, and S. Takahashi, J. Vac. Sci. Technol. A **3**, 1502 (1985); Surf. Sci. **164**, 367 (1985).
[40] G.-X. Qian and D.J. Chadi, Phys. Rev. B **35**, 1288 (1987).
[41] R.S. Becker, B.S. Swartzentruber, J.S. Vickers, and T. Klitsner, Phys. Rev. B **39**, 1633 (1989).
[42] N. Takeuchi, A. Selloni, and E. Tosatti, Phys. Rev. Lett. **69**, 648 (1992).
[43] M. Koike, Y. Einaga, H. Hirayama, and K. Takayanagi, Phys. Rev. B **55**, 15444 (1997).
[44] N. Takeuchi, Phys. Rev. B **57**, 6255 (1998).
[45] G. Kresse and J. Furthmüller, Comput. Mater. Sci. **6**, 15 (1996); Phys. Rev. B **54**, 11169 (1996).
[46] J. Furthmüller, P. Käckell, F. Bechstedt, and G. Kresse, Phys. Rev. B **61**, 4576 (2000).
[47] A. Zywietz, J. Furthmüller, and F. Bechstedt, Phys. Rev. B **59**, 15166 (1999).
[48] H.J. Monkhorst and J.B. Pack, Phys. Rev. B **13**, 518 (1976).
[49] M.S. Hybertsen and S.G. Louie, Phys. Rev. B **34**, 5390 (1986).
[50] F. Bechstedt, Adv. Solid State Phys. **32**, 161 (1992).
[51] U. Starke, J. Schardt, J. Bernhardt, M. Franke, K. Reuter, H. Wedler, K. Heinz, J. Furthmüller, P. Käckell, and F. Bechstedt, Phys. Rev. Lett. **80**, 758 (1998).
[52] J. Furthmüller, P. Käckell, F. Bechstedt, A. Fissel, K. Pfennighaus, B. Schröter, and W. Richter, J. Electron. Mater. **27**, 848 (1998).
[53] J. Furthmüller, F. Bechstedt, H. Hüsken, B. Schröter, and W. Richter, Phys. Rev. B **58**, 13712 (1998).
[54] K. Shiraishi, J. Phys. Soc. Jpn. **59**, 3455 (1990).
[55] F. Bechstedt, W.G. Schmidt, and A. Scholze, Europhys. Lett. **35**, 585 (1996).
[56] H.J. Gossmann, J.C. Bean, L.C. Feldman, E.G. McRae, and I.K. Robinson, Phys. Rev. Lett. **55**, 1106 (1985).
[57] P. Molinas-Mata, A.J. Mayne, and G. Dujardin, Phys. Rev. Lett. **80**, 3101 (1998).
[58] U. Grossner, J. Furthmüller, and F. Bechstedt, Phys. Rev. B **58**, R1722 (1998).
[59] S.Y. Tong, H. Huang, C.M. Wei, W.E. Packard, F.K. Men, G. Glander, and M.B. Webb, J. Vac. Sci. Technol. A **6**, 615 (1988).
[60] R.J. Hamers, R.M. Tromp, and J.E. Demuth, Phys. Rev. Lett. **56**, 1972 (1986).
[61] T. Uchihashi, Y. Sugawara, T. Tsukamoto, M. Ohta, S. Morita, and M. Suzuki, Phys. Rev. B **56**, 9834 (1997).
[62] S.H. Ke, T. Uda, and K. Terakura, Phys. Rev. B **62**, 15319 (2000).
[63] F. Bechstedt and R. Enderlein, *Semiconductor Surfaces and Interfaces* (Akademie-Verlag, Berlin, 1988).
[64] K.D. Brommer, M. Galván, A. Dal Pino, and J.D. Joannopoulos, Surf. Sci. **314**, 57 (1994).